Progress In Electromagnetics Research, Vol. 106, 335–347, 2010

PLASMONIC RESONANT LIGHT SCATTERING BY A CYLINDER WITH RADIAL ANISOTROPY

Y. W. Jin, D. L. Gao, and L. Gao

Jiangsu Key Laboratory of Thin Films
Department of Physics
Soochow University
Suzhou 215006, China

Abstract—We apply the full-wave electromagnetic theory to study electromagnetic scattering by a small cylindrical particle with radial anisotropy for normally incident light with transverse magnetic (TM) polarization. The scattering coefficients are derived, when the radial anisotropies in both the permittivity and permeability tensors are taken into account. It is shown that the surface and volume plasmon resonances can be identified by the sign of $d\varepsilon_t/dq$, in which ε_t is the permittivity element in a direction tangential to the local r-axis, and q is the size parameter. The near field distributions for surface and volume modes are illustrated by finite element method. It is found that small changes of anisotropy can affect the scattering efficiencies significantly. Moreover, the quadrupole and octupole resonant peaks may be much higher and sharper than those of dipole resonance in the scattering efficiency spectra.

1. INTRODUCTION

Light scattering by a small particle is one of the most fundamental problems in electrodynamics [1, 2]. Nowadays it attracts much attention because of the development of the transformation optics [3, 4], which can reroute the light without scattering in the presence of the object according to the invariance of the Maxwell's equations. Analytical methods based on Maxwell's equations have been used to reveal the nature of invisibility cloaks and characterize the wave interaction [5, 6]. Those cloaks are usually made of radially anisotropic

Received 6 June 2010, Accepted 16 July 2010, Scheduled 26 July 2010
Corresponding author: L. Gao (leigao@suda.edu.cn).

and inhomogeneous materials. Later, spherical cloaks with isotropic multi-layer structure were also investigated [7–9]. On the other hand, the localized surface plasmon resonance related to nano-scale metal particles is another key topic in light scattering, which may lead to potential applications in information processing, nanotechnology and engineering [10].

Generally, for spherical particles with the size much smaller than the incident wavelength, Rayleigh theory based on the dipole approximation can be adopted to study the light scattering. However, for a small sphere with weak dissipation near plasmon resonant frequencies, based on the Mie full-wave electromagnetic theory [11–14], the scattering can strongly deviate from Rayleigh scattering and is characterized by very anomalous properties [1, 15, 16]. These anomalous properties include sharp giant optical resonances, enhanced scattering cross sections, complicated energy circulation, the increase of extinction cross section with increasing the order of resonance, etc. More recently, enhanced scattering efficiencies for spherical particles with weakly dissipating anisotropic materials were investigated n Refs. [17, 18].

For small cylindrical nanowire, similar light scattering was predicted according to full-wave electromagnetic solution [19]. In general, for a small isotropic cylinder with the permittivity ε, the excitation of the corresponding surface localized electromagnetic mode takes place under the resonant condition $\varepsilon = -\varepsilon_h$ (ε_h is the permittivity of the surrounding medium). In other words, when the frequency of the eigenmode equals the one for the incident light, the localized surface plasmons can be emitted.

In this paper, we will focus on the light scattering by a radially anisotropic cylinder embedded in free space. The radial anisotropy here means that the permittivity tensor $\overleftrightarrow{\varepsilon}$ is diagonal in cylindrical coordinates (r, θ, z), and the dielectric element along the radial direction differs from the one along tangential direction. In this situation, the permittivity (or/and permeability) tensor(s) of the material are homogeneous and anisotropic in cylindrical coordinates, which are distinguished from those inhomogeneous parameters designed from coordinate transformation [3, 4]. In addition, radial anisotropy is also different from the Cartesian anisotropy [20, 21]. If one transfers the permittivity (or/and permeability) tensor(s) from the cylindrical coordinates to Cartesian coordinates, the parameters would be tensors as well. Moreover, the elements in the 3×3 matrix would all depend on the positions (x, y, z), and there are also off-diagonal elements in the matrix. Actually, such special radial anisotropy can be realized by graphitic multishell structures [22],

spherically stratified medium [23]. We note that a system of anisotropic layers, which consist of closely packed uniform cylinders with permittivity tensor under Cartesian coordinates, was studied as an optical model of the eye cornea [24]. Here we would like to establish the full-wave electromagnetic theory for the radially anisotropic cylinders and investigate the resonant scattering in detail.

Now we turn to the body of the paper. In Section 2, we obtain the wave equations for the cylinder with both dielectric and magnetic anisotropies. The scattering coefficients are determined by the boundary conditions, and the far-field solution is given. Numerical and simulation results for both far-field and near-field are shown in Section 3. The paper ends with a conclusion in Section 4.

2. FORMALISM

We consider the electromagnetic (EM) wave scattering from a radially anisotropic cylinder with radius a as shown in Fig. 1. For simplicity, our analysis is for the normal incidence, i.e., the wave vector $\mathbf{k}$ is perpendicular to the z axis. And the EM wave is assumed to have transverse magnetic (TM) polarization, i.e., the magnetic field only exists in the z direction. The constitutive tensors of the relative permittivity and permeability inside the cylindrical domain are expressed as in cylindrical coordinates,

$$\overleftrightarrow{\varepsilon} = \begin{pmatrix} \varepsilon_r & 0 & 0 \\ 0 & \varepsilon_t & 0 \\ 0 & 0 & \varepsilon_z \end{pmatrix} \quad \text{and} \quad \overleftrightarrow{\mu} = \begin{pmatrix} \mu_r & 0 & 0 \\ 0 & \mu_t & 0 \\ 0 & 0 & \mu_z \end{pmatrix}, \tag{1}$$

where $\varepsilon_r(\mu_r)$ and $\varepsilon_t(\mu_t)$ stand for the permittivity (permeability) elements in a direction parallel (perpendicular or tangential) to the local r-axis, respectively, and $\varepsilon_z(\mu_z)$ corresponds to the element in

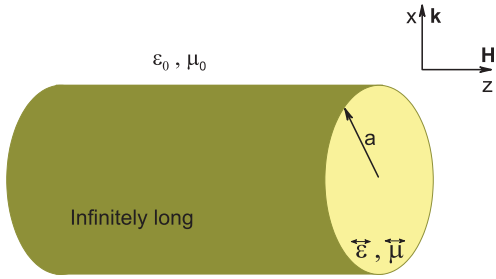

Figure 1. Geometry of an anisotropic cylinder. The incident wave propagates in the direction of $\mathbf{k}$.

a direction parallel to z axis [25]. For a harmonic electromagnetic wave, the time dependence is assumed to be $\sim e^{-i\omega t}$. With Maxwell equations, the time-independent parts of local electric and magnetic fields are written as

$$\nabla \times \mathbf{H} = -i\omega\varepsilon_0 \overleftrightarrow{\varepsilon} \mathbf{E} \quad \text{and} \quad \nabla \times \mathbf{E} = i\omega\mu_0 \overleftrightarrow{\mu} \mathbf{H}. \tag{2}$$

In the cylindrical coordinates, Eq. (2) becomes

$$\begin{cases} \frac{1}{r}\frac{\partial H_z}{\partial \theta} - \frac{\partial H_\theta}{\partial z} = -i\omega\varepsilon_0\varepsilon_r E_r, \\ \frac{\partial H_r}{\partial z} - \frac{\partial H_z}{\partial r} = -i\omega\varepsilon_0\varepsilon_t E_\theta, \\ \frac{1}{r}\frac{\partial}{\partial r}(rH_\theta) - \frac{1}{r}\frac{\partial H_r}{\partial \theta} = -i\omega\varepsilon_0\varepsilon_z E_z, \end{cases} \tag{3}$$

and

$$\begin{cases} \frac{1}{r}\frac{\partial E_z}{\partial \theta} - \frac{\partial E_\theta}{\partial z} = i\omega\mu_0\mu_r H_r, \\ \frac{\partial E_r}{\partial z} - \frac{\partial E_z}{\partial r} = i\omega\mu_0\mu_t H_\theta, \\ \frac{1}{r}\frac{\partial}{\partial r}(rE_\theta) - \frac{1}{r}\frac{\partial E_r}{\partial \theta} = i\omega\mu_0\mu_z H_z. \end{cases} \tag{4}$$

For TM mode, we have $H_\theta = 0$ and $H_r = 0$. As a consequence, Eq. (3) is simplified as

$$\begin{cases} E_r = -\frac{1}{i\omega\varepsilon_0\varepsilon_r}\frac{1}{r}\frac{\partial H_z}{\partial \theta}, \\ E_\theta = \frac{1}{i\omega\varepsilon_0\varepsilon_t}\frac{\partial H_z}{\partial r}, \\ E_z = 0. \end{cases} \tag{5}$$

From Eq. (5), we have

$$\frac{1}{r}\left[\frac{\partial}{\partial r}\left(\frac{r}{\varepsilon_t}\frac{\partial H_z}{\partial r}\right)\right] + \frac{1}{r^2}\frac{\partial}{\partial \theta}\left(\frac{1}{\varepsilon_r}\frac{\partial H_z}{\partial \theta}\right) + k_0^2\mu_z H_z = 0. \tag{6}$$

If we separate variables by using $H_z = \Psi(r)\Theta(\theta)$, Eq. (6) can be decomposed into

$$\frac{d^2\Theta}{d\theta^2} + m^2\Theta = 0, \tag{7}$$

and

$$\frac{d^2\Psi}{dr^2} + r\frac{d\Psi}{dr} + \left(k_0^2\varepsilon_t\mu_z r^2 - m^2\frac{\varepsilon_t}{\varepsilon_r}\right)\Psi = 0, \tag{8}$$

where m is an integer. It is evident that the solution to Eq. (7) is $e^{im\theta}$, and Eq. (8) is a second-order homogeneous differential equation for Ψ. For the incident TM wave, the field H_z can be expanded as $H_z = \sum_{m=-\infty}^{\infty} (i)^m J_m(k_0 r) e^{im\theta}$. Then, the local field solutions in the

inner and outer regions of the cylinder are described as,

$$H_z^{in} = \sum_{m=-\infty}^{\infty} i^m A_m J_{m'}(kr) e^{im\theta}, \quad r < a, \tag{9}$$

$$H_z^{out} = \sum_{m=-\infty}^{\infty} i^m [J_m(k_0 r) + B_m H_m^{(1)}(k_0 r)] e^{im\theta}, \quad r > a, \tag{10}$$

where $m'^2 = m^2 \varepsilon_t / \varepsilon_r$, $k = k_0 \sqrt{\varepsilon_t \mu_t}$ and $k_0 = \omega \sqrt{\varepsilon_0 \mu_0}$. In addition, J_m is mth-order Bessel function, and $H_m^{(1)}$ is the Hankel function of the first kind which represents the outward-traveling cylindrical wave. Physically, J_m and $H_m^{(1)}$ terms for $r > a$ correspond to the incident and scattered waves respectively. To solve the scattering problem, the amplitudes A_m and B_m now become the most important issue. According to the continuous boundary conditions for E_θ and H_z at $r = a$, we obtain,

$$B_m = -\frac{\sqrt{\varepsilon_t \mu_z} J_{m'}(\sqrt{\varepsilon_t \mu_z} q) J_m'(q) - \mu_z J_m(q) J_{m'}'(\sqrt{\varepsilon_t \mu_z} q)}{\sqrt{\varepsilon_t \mu_z} J_{m'}(\sqrt{\varepsilon_t \mu_z} q) H_m^{(1)'}(q) - \mu_z J_{m'}'(\sqrt{\varepsilon_t \mu_z} q) H_m^{(1)}(q)}. \tag{11}$$

Here, we introduce a size parameter $q = k_0 a$. Unlike the situation in isotropic case [19], the coefficient for anisotropic case is asymmetrical, i.e., $B_{-m} \neq B_m$. Incidentally, it is evident that the scattering coefficient B_m reduces to the isotropic case by replacing $\varepsilon_r(\varepsilon_t)$ and $\mu_z(\mu_t)$ with ε and μ, respectively [11].

For the case of far field, the scattering efficiency of a circular cylinder can be expressed by B_m [11, 14, 15, 19],

$$Q_{sca} = \frac{2}{q} \sum_{m=-\infty}^{\infty} |B_m|^2. \tag{12}$$

To explain the optical plasmon resonances, let us express the amplitude as $B_m = -\Re_m / (\Re_m + i\Im_m)$ [1], and we have

$$\Re_m = \sqrt{\varepsilon_t \mu_z} J_{m'}(\sqrt{\varepsilon_t \mu_z} q) J_m'(q) - \mu_z J_m(q) J_{m'}'(\sqrt{\varepsilon_t \mu_z} q), \tag{13}$$

$$\Im_m = \sqrt{\varepsilon_t \mu_z} J_{m'}(\sqrt{\varepsilon_t \mu_z} q) Y_m'(q) - \mu_z J_{m'}'(\sqrt{\varepsilon_t \mu_z} q) Y_m(q), \tag{14}$$

where Y_m is Neumann function. The exact optical resonance corresponds to the situation when $\Im_m = 0$, which leads to the scattering coefficient $|B_m| = 1$. For simplicity, the material is assumed to be nonmagnetic, i.e., $\mu_z = 1$. As a consequence, the solutions for equation $\Im_m = 0$ are only relative to dielectric anisotropy ε_r and ε_t.

In long-wavelength limit $k_0 a \ll 1$ and $k_0 a \sqrt{\varepsilon_t \mu_z} \ll 1$, one can resort to effective medium theory. In this situation, the effective scattering width of the cylinder is determined by $m = 0$ and

$m = 1$ terms [26, 27]. Note that for incident TM wave, the effective permittivity and permeability are still isotropic for radial anisotropy [28, 29]. To search for the effective responses for the radially anisotropic cylinder, one always assumes that the cylinder is embedded in an effective medium with isotropic effective permittivity ε_{eff} and permeability μ_{eff}. In this sense, we replace ε_0 and μ_0 with ε_{eff} and μ_{eff}, and they can be determined when B_0 and B_1 vanish. It requires

$$k_0 J_0(ka) J_0'(k_0 a) - \frac{1}{\varepsilon_t} k J_0(k_0 a) J_0'(ka) = 0, \tag{15}$$

and

$$k_0 J_\nu(ka) J_1'(k_0 a) - \frac{1}{\varepsilon_t} k J_1(k_0 a) J_\nu'(ka) = 0, \tag{16}$$

here $\nu = \sqrt{\varepsilon_t/\varepsilon_r}$. Under the condition that $k_0 a \ll 1$ and $k_0 a \varepsilon_t \mu_z \ll 1$, we can use the following approximation:

$$J_0(x) \cong 1, \quad J_0'(x) \cong -x/2, \quad J_1(x) \cong \frac{x}{2}, \quad J_1'(x) \cong \frac{1}{2}, \quad \text{as } x \to 0$$

As a result, we have

$$\mu_{eff} = 1 \quad \text{and} \quad \varepsilon_{eff} = \sqrt{\varepsilon_r}\sqrt{\varepsilon_t}. \tag{17}$$

By considering the equivalence to the isotropy case, for $q \to 0$, we find that the surface resonant condition tends to be $\sqrt{\varepsilon_r}\sqrt{\varepsilon_t} = -1$, i.e., $\varepsilon_t = 1/\varepsilon_r$ for negative ε_r.

3. THEORETICAL CALCULATIONS

According to above theoretical analysis, the exact plasmon resonance appears when $\Im_m = 0$, which results in real and finite values $|B_m| = 1$ at the resonance frequencies in both isotropic and anisotropic cases [15–17, 19]. For a metallic cylinder, there are two different branches of optical resonances [15, 19]. The first branch is for broad volume resonances, which associates with the excitation of volume waves from the cylindrical cavity (we call them volume modes). The other branch appears at small size parameters, which is associated with excitation of surface plasmons. Thus, we call them surface plasmon resonances or surface modes.

For TM polarization on the anisotropic cylinder, when $\varepsilon_t < 0$, all amplitudes tend to zero at small size parameters q for monopole mode $m = 0$ and they tend to 1 at certain large q, which characterizes the volume resonances (see Fig. 2(a)). However, for dipole mode $m = 1$, in addition to the volume resonances at large q, the surface plasmon resonances arise at small q, which are extremely sharp (see Fig. 2(b)).

As a matter of fact, the surface modes take place for all $m > 0$ modes such as dipole, quadrupole, octopole, etc. From Fig. 2(b), we can also observe that the dielectric anisotropy has more influence on surface plasmon resonances than on volume resonances. For instance, the

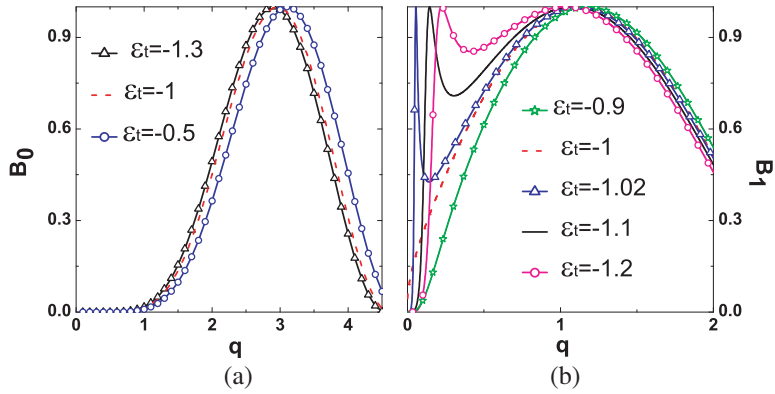

Figure 2. Amplitudes B_m versus size parameter q for $\varepsilon_r = -1$. (a) For monopole mode $m = 0$, the amplitude B_0 only has one peak for large q, which corresponds to the volume resonance. (b) For dipole mode $m = 1$, B_1 has two resonant peaks. One at small q is related to surface plasmon resonance, and the other at large q is for the volume resonance. Note that the red dashed line is for the isotropic case in both two figures.

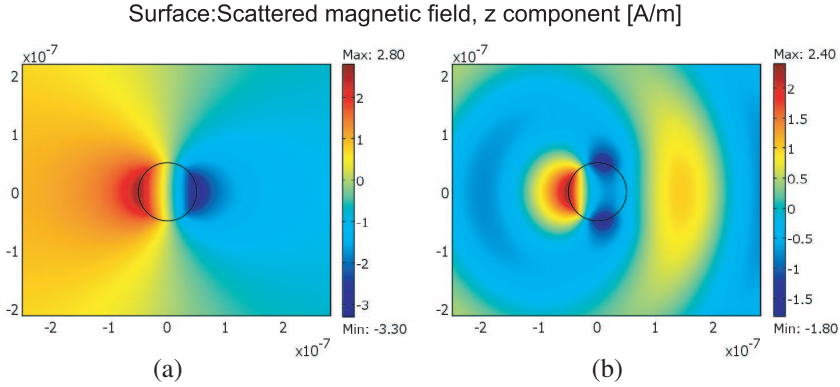

Figure 3. Scattered magnetic field distribution. The radius of the cylinder is 50 nm, and the plane wave propagates from left to right. $\varepsilon_r = -1$ and $\varepsilon_t = -1.1$. (a) The incident Wavelength $\lambda = 2.165 \times 10^{-6}$ m, i.e., $q = 0.145$ for the surface resonant mode; (b) $\lambda = 2.9 \times 10^{-7}$ m, or $q = 1.08$ for the volume resonance.

corresponding q of the surface plasmon resonances increases with the decrease of ε_t, while the positions of volume resonances move to smaller q slightly. In other words, for surface modes, we have $d\varepsilon_t/dq < 0$, while $d\varepsilon_t/dq > 0$ for volume modes. By using the COMSOL Multiphysics based on finite element method, we simulate the near-field scattered magnetic field distribution in the vicinity of the optical resonance. For surface modes, the field is enhanced in the forward and backward directions of light propagation, which are localized on the particle surface, as shown in Fig. 3(a); while for the volume modes, the field distributes around the whole cylinder, as shown in Fig. 3(b).

In order to further investigate volume and surface modes, we plot the trajectories of the resonances on the plane of parameters $\{\varepsilon_t, q\}$ in Fig. 4. According to the sign of $d\varepsilon_t/dq$, one can easily identify the surface plasmon resonant modes and volume resonant modes. Again, we find that there are no surface resonances in monopole modes, while volume modes and surfaces modes coexist for the modes $m \geq 1$. At $q \to 0$, these resonances occur at $\varepsilon_t = 1/\varepsilon_r$, which is different from the condition for isotropic cylinder $\varepsilon = -1$ and the one $\varepsilon = \varepsilon_m = -(m+1)/m$ for spherical particle [15]. The condition $\sqrt{\varepsilon_t}\sqrt{\varepsilon_t} = 1$ can be analytically derived from effective medium theory, which has been discussed in Section 2. From Fig. 4, we again demonstrate that only volume resonances occur at large q for $\varepsilon_t < 0$ and $m = 0$ mode, and both surface plasmon resonances and volume resonances may exist under the condition $\varepsilon_t < 1/\varepsilon_r$ for $m \geq 1$.

In what follows, we study the scattering efficiencies Q_{sca} as a function of q for different ε_t in Fig. 5. A small variation of anisotropy

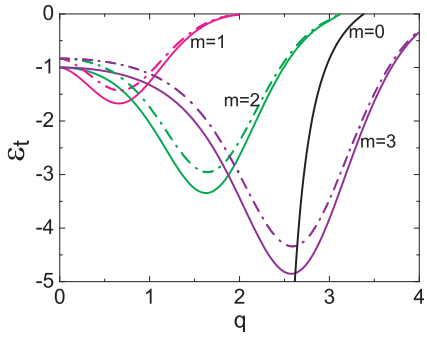

Figure 4. The trajectories of optical resonances for $m = 0$, 1, 2, and 3 by solving the equation $\Im_m = 0$. Volume modes exist in all orders, while surface modes vanish for the monopole case $m = 0$. Solid lines are for $\varepsilon_r = -1$, which merge at $\varepsilon_t = -1$ for the cases $m \geq 1$; and dashed lines are for $\varepsilon_r = -1.2$.

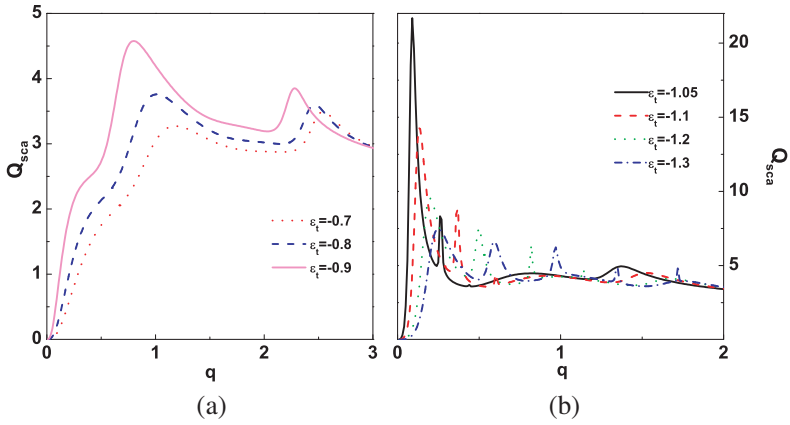

Figure 5. Scattering efficiencies Q_{sca} versus size parameter q for $\varepsilon_r = -1$ and different values of ε_t. (a) For $1/\varepsilon_r < \varepsilon_t < 0$, only volume modes exist. (b) For $\varepsilon_t < 1/\varepsilon_r$, both volume and surface modes exist.

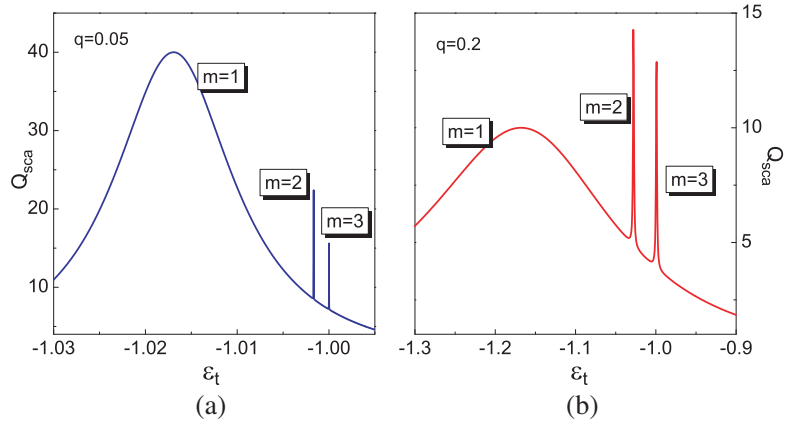

Figure 6. Spectral dependencies of scattering efficiencies for various q. (a) $q = 0.05$ and (b) $q = 0.2$.

parameter leads to quite different scattering efficiencies. One can observe that for $\varepsilon_t > 1/\varepsilon_r$ (see Fig. 5(a)), the peaks for each resonance are not very sharp. This is due to the fact that only volume resonances occur in this range (see in Fig. 4). On the other hand, one can see new multiple resonances with $\varepsilon_t < 1/\varepsilon_r$ in Fig. 5(b), which have sharp resonance peaks. There are multiple peaks corresponding to different resonant orders and size parameter q. Note that the dramatic change of the Q_{sca} spectrum from Fig. 5(a) to 5(b) is caused by small variation in anisotropy parameter. Therefore, a small variation in the

radial anisotropy may result in enhancing or prohibiting scattering efficiencies.

In the end, for the sake of the discussion about influence of the radial anisotropy, we discuss the relation between Q_{sca} and ε_t. From Fig. 6, we find that for $q = 0.2$, the quadrupole and octupole resonances are not suppressed as expected, instead, the corresponding resonant peaks may be much higher than that of dipole resonance. Moreover, the quadrupolar and octupolar peaks in the spectrum Q_{sca} versus anisotropy parameter ε_t are extremely sharp (see Fig. 6(b)). This can be related to the anomalous light scattering due to weak dissipation and at surface plasmon resonances [15].

4. CONCLUSION

We establish the full-wave electromagnetic wave theory to investigate the properties of the light scattering from a radially anisotropic cylinder. It is found that the scattering efficiency is dramatically affected by the radial anisotropy especially near the surface plasmon resonance. When $\varepsilon_t < \frac{1}{\varepsilon_r}$, the surface plasmon resonances may arise at small q for $m \geq 1$, while volume resonances may occur at large q. Volume modes and surface modes can be identified by the sign of $d\varepsilon_t/dq$. In addition, for the scattering efficiency spectrum with $q \ll 1$, the quadrupole and octupole resonant peaks may be much higher and sharper than that of dipole resonance. The study of optical scattering and near-field spectra by nanocylinders may be important for various modern applications such as plasmonic nanolithography, astigmatic optical tweezers, near-field optical microscopy, nonlinear optics in nanowires, etc. [19]. In addition, the sensitivity of far-field quantities such as the scattering efficiency to the radial anisotropy may be used for several potential applications including remote controlling, designing sensors, and enhancing the quality of confocal laser scanning microscopy images [30], etc.

ACKNOWLEDGMENT

We thank Dr. Cheng-Wei Qiu for his stimulating suggestions and comments. This work was supported by the Key Project in Science and Technology Innovation Cultivation Program of Soochow University and the Plan of Dongwu Scholar.

REFERENCES

1. Tribelsky, M. I. and B. S. Luk'yanchuk, "Anomalous light scattering by small particles," *Phys. Rev. Lett.*, Vol. 97, 263902, 2006.
2. Maier, S. A., *Plasmonics: Fundamentals and Applications*, Springer, New York, 2007.
3. Leonhardt, T., "Optical conformal mapping," *Science,* Vol. 312, 1777–1780, 2006.
4. Pendry, J. B., D. Schurig, and D. R. Smith, "Controlling electromagnetic fields," *Science,* Vol. 312, 1780–1782, 2006.
5. Chen, H. S., B.-I. Wu, B. L. Zhang, and J. A. Kong, "Electromagnetic wave interactions with a metamaterial cloak," *Phys. Rev. Lett.,* Vol. 99, 063903, 2007.
6. Qiu, C. W., A. Novitsky, H. Ma, and S. B. Qu, "Electromagnetic interaction of arbitrary radial-dependent anisotropic spheres and improved invisibility for nonlinear-transformation-based cloaks," *Phys. Rev. E,* Vol. 80, 016604, 2009.
7. Qiu, C. W., L. Hu, X. Xu, and Y. Feng, "Spherical cloaking with homogeneous isotropic multilayered structures," *Phys. Rev. E,* Vol. 79, 047602, 2009.
8. Cheng, Y. and X. J. Liu, "Three dimensional multilayered acoustic cloak with homogeneous isotropic materials," *Appl. Phys. A,* Vol. 94, 25–30, 2009.
9. Qiu, C. W., L. Hu, B. Zhang, B. Wu, S. Johnson, and J. Joannopoulos, "Spherical cloaking using nonlinear transformations for improved segmentation into concentric isotropic coatings," *Opt. Express,* Vol. 17, 13467–13478, 2009.
10. Khlebtsov, N. G., "Optics and biophotonics of nanoparticles with a plasmon resonance," *Quantum Electron.,* Vol. 38, 504–529, 2008.
11. Hulst, V. D., *Light Scattering by Small Particles*, Dover, New York, 2000.
12. Kerker, M., *The Scattering of the Light and Other Electromagnetic Radiation*, Academic Press, New York, 1969.
13. Bohren, C. F. and D. R. Huffman, *Absorption and Scattering of Light by Small Particles*, Willey, New York, 1983.
14. Born, M., *Principles of Optics*, 2nd edition, University Press, Cambridge, 1999.
15. Luk'yanchuk, B. S. and M. I. Tribelsky, "Peculiarities of light scattering by nanoparticles and nanowires near plasmon resonance frequencies in weakly dissipating materials," *J. Opt. A: Pure Appl.*

Opt., Vol. 9, S294–S300, 2007.

16. Luk'yanchuk, B. S. and M. I. Tribelsky, "Extraordinary scattering diagram for nanoparticles near plasmon resonance frequencies," *Appl. Phys. A,* Vol. 89, 259–264, 2007.
17. Luk'yanchuk, B. S. and C. W. Qiu, "Enhanced scattering efficiencies in spherical particles with weakly dissipating anisotropic materials," *Appl. Phys. A,* Vol. 92, 773–776, 2008.
18. Qiu, C. W. and B. S. Luk'yanchuk, "Peculiarities in light scattering by spherical particles with radial anisotropy," *J. Opt. Soc. Am. A,* Vol. 25, 1623–1628, 2008.
19. Luk'yanchuk, B. S. and V. Ternovsky, "Light scattering by a thin wire with a surface-plasmon resonance: Bifurcations of the poynting vector field," *Phys. Rev. B,* Vol. 73, 235432, 2006.
20. Monzon, J. C., "Two-dimensional scattering by a homogeneous anisotropic rod," *IEEE Trans. Antennas Propag.*, Vol. 34, 1243–1249, 1986.
21. Ren W., X. B. Wu, Z. Yi, and W. G. Lin, "Properties of wave functions in homogeneous anisotropic media," *Phy. Rev. E,* Vol. 51, 671–679, 1995.
22. Lucas, A. A., L. Henrard, and Ph. Lambin, "Computation of the ultraviolet absorption and electron inelastic scattering cross section of multishell fullerenes," *Phys. Rev. B,* Vol. 49, 2888–2896, 1994.
23. Sten, J. C. E., "DC fields and analytical image solutions for a radially anisotropic spherical conductor," *IEEE Trans. Dielectr. Electr. Insul.*, Vol. 2, 360–367, 1995.
24. Izotova, V. F., I. L. Maksimova, I. S. Nefedov, and S. V. Romanov, "Investigation of Mueller matrices of anisotropic nonhomogeneous layers in application to an optical model of the cornea," *Appl. Optics*, Vol. 36, 164–169, 1997.
25. Henrard, L. and P. Lambin, "Calculation of the eneregy loss for an electron passing near giant fullerenes," *J. Phys. B,* Vol. 29, 5127–5141, 1996.
26. Wu, Y., J. S. Li, Z. Q. Zhang, and C. T. Chan, "Effective medium theory for magnetodielectric composites: Beyond the long-wavelength limit," *Phys. Rev. B,* Vol. 74, 085111, 2006.
27. Gao, L., T. H. Fung, K. W. Yu, and C. W. Qiu, "Electromagnetic transparency by coated spheres with radial anisotropy," *Phys. Rev. E,* Vol. 78, 046609, 2008.
28. Gao, L. and X. Yu, "Optical bistability in nonlinear mixtures of coated inclusions with radial dielectric anisotropy," *Phys. Lett. A,*

Vol. 335, 457–463, 2005.

29. Yu, X. P. and L. Gao, "Nonlinear dielectric response in partially resonant composites with radial dielectric anisotropy," *Phys. Lett. A,* Vol. 359, 516–522, 2006.
30. Lemelle, A., B. Veksler, I. S. Kozhevnikov, G. G. Akchurin, S. A. Piletsky, and I. Meglinski, "Application of gold nanoparticles as contrast agents in confocal laser scanning microscopy," *Laser Phys. Lett.*, Vol. 6, 71–75, 2009.